Inorg. Chem. **2007**, *46*, 884–895

Structural, Spectral, Electric-Field-Induced Second Harmonic, and Theoretical Study of Ni(II), Cu(II), Zn(II), and VO(II) Complexes with $[N_2O_2]$ Unsymmetrical Schiff Bases of *S*-Methylisothiosemicarbazide Derivatives†

Julieta Gradinaru,‡ Alessandra Forni,*,§ Vadim Druta,‡ Francesca Tessore,|| Sandro Zecchin,⊥ Silvio Quici,§ and Nicolae Garbalau‡

Institute of Chemistry of the Academy of Sciences of Moldova, str. Academiei, 3, MD-2028 Chisinau, R. Moldova, CNR-Istituto di Scienze e Tecnologie Molecolari, via Golgi 19, I-20133 Milan, Italy, Department of Inorganic Chemistry, Università degli Studi di Milano and Centro di Eccellenza CIMAINA, via Venezian 21, I-20133 Milano, Italy, and IENI-CNR, Corso Stati Uniti 4, I-35127 Padova, Italy

Received October 24, 2006

New unsymmetrical $[N_2O_2]$ tetradentate Schiff base complexes of Ni(II), Cu(II), Zn(II), and VO(II) were synthesized by template condensation of the tetradentate precursor 1-phenylbutane-1,3-dione mono-*S*-methylisothiosemicarbazone with *o*-hydroxybenzaldehyde or its 5-phenylazo derivative. They were characterized by elemental analysis, IR, UV–vis, electron spin resonance, and NMR spectroscopy, mass spectrometry, and magnetic measurements. The crystal structures of five of them have been determined by X-ray diffraction using, in some cases, synchrotron radiation. These compounds are characterized by a large thermal stability; their decomposition temperatures range from 240 up to 310 °C. Complexes with the phenylazo substituent were found to possess a large second-order nonlinear optical (NLO) response, as determined both by measurements of solution-phase direct current electric-field-induced second harmonic generation and by theoretical time-dependent density functional theory (TDDFT) calculations. The molecular hyperpolarizability was found to decrease in the order Zn(II) > Cu(II) > Ni(II) ∼ VO(II). The active role of the metal in determining the NLO properties of the complexes was shown through an analysis of their UV–vis spectra, which revealed the presence of metal-to-ligand (in closed-shell complexes) and ligand-to-metal (in open-shell complexes) charge-transfer bands together with intra-ligand charge-transfer transitions. Assignment of the bands was based on the analysis of the TDDFT computed spectra.

Introduction

The development of new second-order nonlinear optical (NLO) materials based on transition metal complexes represents an emerging area of research owing to the unique structural and electronic properties associated with organometallic and coordination compounds.[1−3] Among the different classes of transition metal complexes exhibiting potentially large NLO responses, salen-type Schiff base complexes have attracted attention since the early 1990s.[4,5] In such compounds having generally a planar or a pseudoplanar structure, the metal atom is strategically placed at the center

* To whom correspondence should be addressed. E-mail: alessandra.forni@istm.cnr.it.

† This work is dedicated to the memory of Professor Nicolae Garbalau, who passed away on February 20, 2006.

‡ Institute of Chemistry of the Academy of Sciences of Moldova.
§ CNR-Istituto di Scienze e Tecnologie Molecolari.
|| Università degli Studi di Milano.
⊥ IENI-CNR.

(1) (a) Kanis, D. R.; Ratner, M. A.; Marks, T. J. *J. Am. Chem. Soc.* **1992**, *114*, 10338−10357. (b) Coe, B. J.; Curati, N. R. M. *Comments Inorg. Chem.* **2004**, *25*, 147−184. (c) Le Bozec, H.; Renouard, T. *Eur. J. Inorg. Chem.* **2000**, 229−239. (d) Heck, J.; Dabek, S.; Meyer-Friedrichsen, T.; Wong, H. *Coord. Chem. Rev.* **1999**, *190−192*, 1217−1254. (e) Roberto, D.; Tessore, F.; Ugo, R.; Bruni, S.; Manfredi, A.; Quici, S. *Chem. Commun.* **2002**, 846−847.

(2) (a) Long, N. J. *Angew. Chem., Int. Ed. Engl.* **1995**, *34*, 21−38. (b) Powell, C. P.; Humphrey, M. G.; Morrall, M. G.; Samoc, J. P. L.; Luther-Davies, B. J. *Phys. Chem. A* **2003**, *107*, 11264−11266. (c) Whittal, I. R.; McDonagh, A. M.; Humphrey, M. G. *Adv. Organomet. Chem.* **1998**, *42*, 291−362. (d) Coe, B. J. In *Comprehensive Coordination Chemistry II;* McCleverty, J. A., Meyer, T. J., Eds.; Elsevier Pergamon: Oxford, U.K., 2004; Vol. 9, pp 621−687. (e) Cariati, E.; Pizzotti, M.; Roberto, D.; Tessore, F.; Ugo, R. *Coord. Chem. Rev.* **2006**, *250*, 1210−1233.

10.1021/ic062035r CCC: $37.00
Published on Web 01/12/2007

Scheme 1

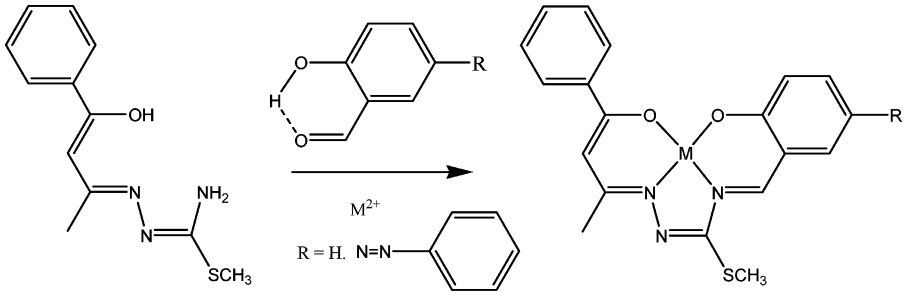

ML^1, R=H, M=Ni^{2+}(**1**), Cu^{2+}(**2**), Zn^{2+}(**3**), VO^{2+}(**4**)

ML^2, R=N_2Ph, M=Ni^{2+}(**5**), Cu^{2+}(**6**), Zn^{2+}(**7**), VO^{2+}(**8**)

of the charge-transfer system, allowing the d electrons of the metal to take part in the conjugation scheme of the organic ligand. As a result, enhanced optical nonlinearities are observed after metal complexation, compared to those of the free ligand. Besides their large NLO responses, these complexes are characterized by exceptionally high stability constants comparable to those of biological receptors making them promising candidates for successful applications in the field of optoelectronic technologies.[6−11]

In recent years, the chemistry of bis(salicylidene)-*S*-alkylisothiosemicarbazone complexes, analogues of salen-type complexes where *S*-alkylisothiosemicarbazide is used as the diamine moiety instead of ethylenediamine, has been thoroughly studied.[12,13] *S*-Alkylisothiosemicarbazide is especially interesting for the assembling of asymmetric systems because of the nonequivalence of its terminal amino groups. Owing to the high activity of the 2-hydroxybenzaldehyde unit, however, preparation of the asymmetric tetradentate monosalicylidene-isothiosemicarbazide species[14−17] is nontrivial. A two-step reaction via "half-unit" precursors appeared to be a promising strategy. To this aim, we have used benzoylacetone *S*-methylisothiosemicarbazone as the half-unit starting block for assembling both cyclic and unsymmetrical open-type species (see Scheme S1 in Supporting Information for a picture of related previous work).[18−21]

Taking into account that bis(salicylaldiminato) complexes possess molecular optical nonlinearities,[3−11,22−26] we have hypothesized that such properties can be exhibited and eventually increased, through proper addition of electron acceptor and/or donor groups, by our thiosemicarbazide-based complexes. We have therefore prepared a new series of Ni, Cu, Zn, and VO complexes with two unsymmetrical tetradentate [N_2O_2] Schiff base ligands (see Scheme 1) obtained by condensation of benzoylacetone *S*-methylisothiosemicarbazone with *o*-hydroxybenzaldehyde (**1**−**4**) or its 5-phenylazo derivative (**5**−**8**). This was done with the purpose of evaluating their NLO response in relation to (i) the architecture itself of these complexes compared, in particular, with that of more conventional push−pull salen-type complexes,[24−26] (ii) the different transition-metal centers considered under the same coordinating scheme, and (iii) the adding of an electron acceptor group, such as the phenylazo unit, onto the starting unsubstituted ligand structure.

We report herein about the synthesis and characterization of these complexes, including the X-ray structure determination for five representatives. The values of the quadratic hyperpolarizability of selected complexes, as measured by the solution-phase direct current (dc) electric-field-induced second harmonic (EFISH) generation, will also be reported together with the results of the density functional theory (DFT) and time-dependent DFT (TDDFT) calculations aimed

(3) Di Bella, S. *Chem. Soc. Rev.* **2001**, *30*, 355−366 and references therein.
(4) Di Bella, S.; Fragalà, I. *Synth. Met.* **2000**, *115*, 191−196.
(5) Lacroix, P. G. *Eur. J. Inorg. Chem.* **2001**, 339−348 and references therein.
(6) Di Bella, S.; Fragalà, I. *New J. Chem.* **2002**, *26*, 285−290.
(7) Di Bella, S.; Fragalà, I.; Ledoux, I.; Diaz-Garcia, M. A.; Lacroix, P. G.; Marks, T. J. *Chem. Mater.* **1994**, *6*, 881−883.
(8) Cariati, F.; Caruso, U.; Centore, R.; Marcolli, W.; De Maria, A.; Panunzi, B.; Roviello, A.; Tuzi, A. *Inorg. Chem.* **2002**, *41*, 6597−6603.
(9) Chiang, W.; Vanengen, D.; Thompson, M. E. *Polyhedron* **1996**, *15*, 2369−2376.
(10) Atkins, R.; Brewer, G.; Kokot, E.; Mockler, G. M.; Sinn, E. *Inorg. Chem.* **1985**, *24*, 127−134.
(11) Averseng, F.; Lacroix, P. G.; Malfant, I.; Lenoble, G.; Cassoux, P.; Nakatani, K.; Maltey-Fenton, I.; Delaire, J. A. *Chem. Mater.* **1999**, *11*, 995−1002.
(12) Gerbeleu, N. V.; Arion, V. B.; Burgess, J. *Template Synthesis of Macrocyclic Compounds;* Wiley−VCH: New York, 1999; p 544.
(13) Arion, V.; Revenco, M.; Gradinaru, J.; Simonov, Y.; Gerbeleu, N.; Saint-Aman, E.; Adams, F. *Rev. Inorg. Chem.* **2001**, *21*, 1−42.
(14) Gerbeleu, N. V.; Arion, V. B.; Simonov, Y. A.; Bourosh, P. N.; Dvorkin, A. A.; Indrichan, K. M. *Zh. Neorg. Khim.* **1990**, *35*, 918−925.
(15) Leovac, V. M.; Divjakovic, V.; Cesljevic, V. I.; Engel, P. *Polyhedron* **1987**, *6*, 1901−1907.
(16) Leovac, V. M.; Jovanovic, L. S.; Bjelica, L. J.; Cesljevic, V. I. *Polyhedron* **1989**, *8*, 135−141.
(17) Cesljevic, V. I.; Leovac, V. M. *J. Serb. Chem. Soc.* **1994**, *59*, 13−19.
(18) Gradinaru, J.; Simonov, Y.; Arion, V.; Bourosh, P.; Popovici, M.; Bel'skii, V.; Gerbeleu, N. *Inorg. Chim. Acta* **2001**, *313*, 30−36.
(19) Gradinaru, J.; Forni, A.; Druta, V.; Quici, S.; Britchi, A.; Deleanu, C.; Gerbeleu, N. *Inorg. Chim. Acta* **2002**, *338*, 169−181.
(20) Forni, A.; Gradinaru, J.; Druta, V.; Zecchin, S.; Quici, S.; Gerbeleu, N. *Inorg. Chim. Acta* **2003**, *353*, 336−343.
(21) Gradinaru, J.; Forni, A.; Simonov, Y.; Popovici, M.; Zecchin, S.; Gdaniec, M.; Fenton, D. *Inorg. Chim. Acta* **2004**, *357*, 2728−2736.
(22) Lenoble, G.; Lacroix, P. G.; Daran, J. C.; Di Bella, S.; Nakatani, K. *Inorg. Chem.* **1998**, *37*, 2158−2165.
(23) Lacroix, P. G.; Di Bella, S.; Ledoux, I. *Chem. Mater.* **1996**, *8*, 541−545.
(24) Di Bella, S.; Fragalà, I.; Ledoux, I.; Marks, T. J. *J. Am. Chem. Soc.* **1995**, *117*, 9481−9485.
(25) Di Bella, S.; Fragalà, I.; Ledoux, I.; Diaz-Garcia, M. A.; Marks, T. J. *J. Am. Chem. Soc.* **1997**, *119*, 9550−9557.
(26) Rigamonti, L.; Demartin, F.; Forni, A.; Righetto, S.; Pasini, A. *Inorg. Chem.* **2006**, *45*, 10976−10989.

Scheme 2

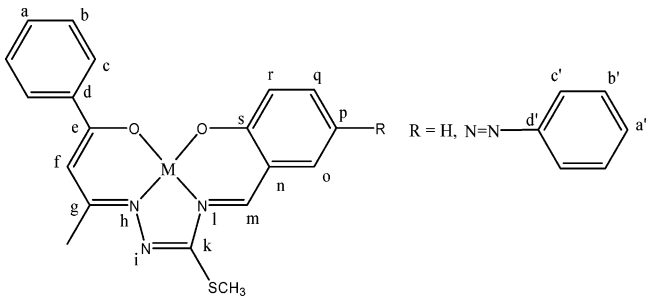

at understanding the origin of the optical properties and, in particular, assigning the electronic transitions of the complexes.

Experimental Section

Materials and Synthesis. All chemicals were of reagent grade and used as commercially purchased without further purification. *S*-Methylisothiosemicarbazide hydroiodide was obtained by reaction of thiosemicarbazide with methyl iodide in dry methanol. Phenylbutane-1,3-dione mono-*S*-methylisothiosemicarbazone (H_2L) was prepared according to literature.[27] Attachment of a phenylazo group on the para position of salicylaldehyde was accomplished by a general azo-coupling method.[28]

A warm solution of $Ni(OAc)_2 \cdot 4H_2O$ (0.25 g, 1.0 mmol) in methanol (10 cm^3) was added to a solution containing phenylbutane-1,3-dione mono-*S*-methylisothiosemicarbazone (0.25 g, 1.0 mmol), salicylaldehyde (0.2 cm^3, 1.5 mmol), and triethylamine (1 cm^3). Precipitation of complex **1** occurred immediately. The precipitate was collected after cooling and washed with methanol and ether. Complexes **2**−**4** were synthesized in a similar way, using as template metal ion sources $Cu(OAc)_2 \cdot 2H_2O$ (0.19 g, 1 mmol), $Zn(OAc)_2 \cdot 2H_2O$ (0.22 g, 1 mmol), and $VOSO_4 \cdot H_2O$ (0.18 g, 1 mmol), respectively.

Compounds **5**−**8** were prepared following the one-pot template procedure as for **1**−**4** but using, instead of salicylaldehyde, the derivative 5-phenylazo-salicylaldehyde (0.23 g, 1.0 mmol).

Single crystals of the complexes were obtained by slow evaporation from a chloroform/methanol (1:1) solution at room temperature.

The atom labeling for ^1H and ^{13}C NMR data for nickel and zinc complexes is reported in Scheme 2. IR data are given as Supporting Information.

Complex NiL^1 (1). [8-(2′-Oxyphenyl)-3-methyl-1-phenyl-6-thiomethyl-1-one-4,5,7-triazaocta-1,3,5,7-tetraenato-(−)-2′-olato-(−)-*O*,*O*′,*N*4,*N*7]nickel(II): yield 0.38 g, 93%. Anal. Calcd for $C_{19}H_{17}N_3NiO_2S$ (fw = 410.12): C, 55.64; H, 4.18; N, 10.25. Found: C, 55.92; H, 4.44; N, 9.98. UV ($CHCl_3$) λ_{max}, nm (ϵ, dm^3 mol^{-1} cm^{-1}): 485 (10 100), 372 (11 900), 346 (13 800), 296 (19 500), 246 (34 700). *m*/*z* = 409 (*I*, 100%). ^1H NMR ($CDCl_3$): δ 2.49 (s, 3H^g, *Me*), 2.71 (s, 3H, *S-Me*), 5.98 (s, 1H^f, C*H*), 6.73 (dd, *J* = 1.5 Hz, *J* = 8.2 Hz, 1H^p, CH_{sal}), 7.24 (d, *J* = 8.9 Hz, 1H^r, CH_{sal}), 7.38−7.45 (m, 2H^{q,o} + 3H^{a,b}, CH_{sal} + CH_{Ph}), 7.90−7.93 (m, 2H^c, CH_{Ph}), 7.96 (s, 1H^m, C*H*═N). ^{13}C NMR ($CDCl_3$): δ 15.92 (C, *S-Me*), 20.10 (C^g, *Me*), 96.93 (C^f, *C*H), 117.16 (C^p, *CH*$_{sal}$), 120.10 (C^n, tert), 123.81 (C^r, *C*H$_{sal}$), 127.59 (C^c, *C*H$_{Ph}$), 128.57 (C^b, *C*H$_{Ph}$), 130.61 (C^a, *C*H$_{Ph}$), 134.27 (C^q, *C*H$_{sal}$), 136.60 (C^o, *C*H$_{sal}$), 137.76 (C^d, tert), 155.22 (C^s, tert), 155.30 (C^m, *C*H═N), 163.02 (C^k, tert), 168.71 (C^g, tert), 174.42 (C^e, tert).

Complex CuL^1 (2). [8-(2′-Oxyphenyl)-3-methyl-1-phenyl-6-thiomethyl-1-one-4,5,7-triazaocta-1,3,5,7-tetraenato-(−)-2′-olato-(−)-*O*,*O*′,*N*4,*N*7]copper(II): yield 0.37 g, 89%. Anal. Calcd for $C_{19}H_{17}CuN_3O_2S$ (fw = 414.97): C, 54.99; H, 4.13; N, 10.13. Found: C, 54.93; H, 4.34; N, 9.83. UV ($CHCl_3$) λ_{max}, nm (ϵ, dm^3 mol^{-1} cm^{-1}): 435 (18 300), 360 (16 800), 311 (25 000), 247 (29 600). *m*/*z* = 414 (*I*, 100%).

Complex ZnL^1 (3). [8-(2′-Oxyphenyl)-3-methyl-1-phenyl-6-thiomethyl-1-one-4,5,7-triazaocta-1,3,5,7-tetraenato-(−)-2′-olato-(−)-*O*,*O*′,*N*4,*N*7]zinc(II): yield 0.38 g, 85%. Anal. Calcd for $C_{19}H_{17}N_3O_2SZn \cdot CH_3OH$ (fw = 448.86): C, 53.52; H, 4.72; N, 9.36. Found: C, 53.17; H, 4.75; N, 9.49. UV ($CHCl_3$) λ_{max}, nm (ϵ, dm^3 mol^{-1} cm^{-1}): 489 (10 900), 419 (10 600), 368 (15 200), 300 (18 000), 280 (12 100). *m*/*z* = 415 (*I*, 100%). ^1H NMR (d_6-DMSO): δ 2.34 (s, 3H^g, *Me*), 2.56 (s, 3H, *S-Me*), 5.72 (s, 1H^f, C*H*), 6.55−6.59 (m, 1H^p, CH_{sal}), 6.78 (d, *J* = 7.9 Hz, 1H^r, CH_{sal}), 7.32−7.37 (m, 1H^q, CH_{sal}), 7.41−7.45 (m, 3H^{a,b}, CH_{Ph}), 7.47 (dd, *J* = 1.8 Hz, *J* = 8.1 Hz, 1H^o, CH_{sal}), 7.91−7.94 (m, 2H^c, CH_{Ph}), 8.56 (s, 1H^m, C*H*═N). ^{13}C NMR (d_6-DMSO): δ 13.36 (C, *S-Me*), 20.97 (C^g, *Me*), 93.77 (C^f, *C*H), 114.89 (C^p, *CH*$_{sal}$), 119.54 (C^n, tert), 124.81 (C^r, *C*H$_{sal}$), 127.48 (C^c, *C*H$_{Ph}$), 128.96 (C^b, *C*H$_{Ph}$), 130.31 (C^a, *C*H$_{Ph}$), 136.93 (C^q, *C*H$_{sal}$), 137.80 (C^o, *C*H$_{sal}$), 142.13 (C^d, tert), 153.41 (C^s, tert), 163.61 (C^m, *C*H═N), 168.40 (C^k, tert), 174.35 (C^g, tert), 177.57 (C^e, tert).

Complex VOL^1 (4). [8-(2′-Oxyphenyl)-3-methyl-1-phenyl-6-thiomethyl-1-one-4,5,7-triazaocta-1,3,5,7-tetraenato-(−)-2′-olato-(−)-*O*,*O*′,*N*4,*N*7]oxovanadium(IV): yield 0.29 g, 69%. Anal. Calcd for $C_{19}H_{17}N_3O_3SV$ (fw = 418.36): C, 54.55; H, 4.10; N, 10.04. Found: C, 54.13; H, 3.88; N, 9.73. UV ($CHCl_3$) λ_{max}, nm (ϵ, dm^3 mol^{-1} cm^{-1}): 475 (9400), 424 (12 200), 386 (17 300), 313 (17 100), 252 (18 500). *m*/*z* = 418 (*I*, 100%).

Complex NiL^2 (5). [8-(2′-Oxy-5′-phenylaza-phenyl)-3-methyl-1-phenyl-6-thiomethyl-1-one-4,5,7-triazaocta-1,3,5,7-tetraenato-(−)-2′-olato-(−)-*O*,*O*′,*N*4,*N*7]nickel(II): yield 0.45 g, 88%. Anal. Calcd for $C_{25}H_{21}N_5NiO_2S$ (fw = 514.23): C, 58.39; H, 4.12; N, 13.63. Found: C, 58.69; H, 4.28; N, 13.46. UV ($CHCl_3$) λ_{max}, nm (ϵ, dm^3 mol^{-1} cm^{-1}): 495 (13 100), 375 (34 000), 294 (20 400), 245 (29 700) . *m*/*z* = 513 (*I*, 100%). ^1H NMR ($CDCl_3$): δ 2.50 (s, 3H^g, *Me*), 2.74 (s, 3H, *S-Me*), 6.01 (s, 1H^f, C*H*), 7.30−7.33 (m, 1H^r, CH_{sal}), 7.39−7.55 (m, 6H$^{a,b,a',b'}$, CH_{Ph}), 7.87−7.94 (m, 4H$^{c,c'}$, CH_{Ph}), 8.11 (s, 1H^m, C*H*═N), 8.14−8.16 (m, 2H^{o,q}, CH_{sal}). ^{13}C NMR ($CDCl_3$): δ 15.98 (C, *S-Me*), 21.06 (C^g, *Me*), 97.13 (C^f, *C*H), 119.63 (C^n, tert), 122.89 (2C$^{c'}$, *CH*$_{Ph}$), 124.86 (C^r, *C*H$_{sal}$), 127.61 (2C^c, *C*H$_{Ph}$), 127.97 (C^o, *C*H$_{sal}$), 128.66 (2C^b, *C*H$_{Ph}$), 129.47 (2C$^{b'}$, *C*H$_{Ph}$), 130.68 (C^a, *C*H$_{Ph}$), 130.81 (C$^{a'}$, *C*H$_{Ph}$), 134.68 (C^q, *C*H$_{sal}$), 137.53 (C^d, tert), 144.16 (C^p, tert), 153.03 (C$^{d'}$, tert), 154.97 (C^s, tert), 155.94 (C^m, *C*H═N), 163.27 (C^k, tert), 170.86 (C^g, tert), 174.66 (C^e, tert).

Complex CuL^2 (6). [8-(2′-Oxy-5′-phenylazo-phenyl)-3-methyl-1-phenyl-6-thiomethyl-1-one-4,5,7-triazaocta-1,3,5,7-tetraenato-(−)-2′-olato-(−)-*O*,*O*′,*N*4,*N*7]copper(II): yield 0.39 g, 75%. Anal. Calcd for $C_{25}H_{21}CuN_5O_2S$ (fw = 519.08): C, 57.85; H, 4.08; N, 13.49. Found: C, 58.01; H, 4.27; N, 13.13. UV ($CHCl_3$) λ_{max}, nm (ϵ, dm^3 mol^{-1} cm^{-1}): 490 (12 800), 448 (14 200), 360 (34 800), 310 (23 300), 245 (27 800). *m*/*z* = 518 (*I*, 28%).

Complex ZnL^2 (7). [8-(2′-Oxy-5′-phenylazo-phenyl)-3-methyl-1-phenyl-6-thiomethyl-1-one-4,5,7-triazaocta-1,3,5,7-tetraenato-(−)-2′-olato-(−)-*O*,*O*′,*N*4,*N*7]zinc(II): yield 0.41 g, 74%. Anal. Calcd for $C_{25}H_{21}N_5O_2SZn \cdot CH_3OH$ (fw = 552.96): C, 56.47; H, 4.56; N, 12.67. Found: C, 56.33; H, 4.58; N, 12.36. UV ($CHCl_3$) λ_{max}, nm (ϵ, dm^3 mol^{-1} cm^{-1}): 479 (13 900), 360 (34 600), 304 (27 300), 242 (15 300). *m*/*z* = 519 (*I*, 100%). ^1H NMR (d_6-DMSO): δ 2.36 (s, 3H^g, *Me*), 2.58 (s, 3H, *S-Me*), 5.75 (s, 1H^f,

(27) Leovac, V. M.; Jovanovic, L. S.; Cesljevic, V. I.; Bjelica, L. J.; Arion, V. B.; Gerbeleu, N. V. *Polyhedron* **1994**, *13*, 3005−3014.
(28) Khandar, A. A.; Rezvani, Z. *Polyhedron* **1998**, *18*, 129−133.

C*H*), 6.91 (d, $J = 9.41$, 1H^{r}, CH_{sal}), 7.41−7.58 (m, 6H$^{a,b,a',b'}$, CH_{Ph}), 7.80−7.82 (m, 2H^{c}, CH_{Ph}), 7.92−7.99 (m, 3H^{q,c1}, 1CH_{sal}, 2CH_{Ph}), 8.28−8.32 (m, 1H^{o}, CH_{sal}), 8.77 (s, 1H, C*H*═N). ^{13}C NMR (d_6-DMSO): δ 13.37 (C, *S-Me*), 20.96 (C^{g}, *Me*), 93.89 (C^{f}, *C*H), 122.73 (C^{c}, *C*H$_{Ph}$), 126.24 (C^{r}, *C*H$_{sal}$), 127.10, 127.50 (C^{q,c1}, *C*H$_{sal}$, *C*H$_{Ph}$), 128.99, 130.19, 130.39, 130.79 (C^{a,b,a1,b1}, *C*H$_{Ph}$), 138.86 (C^{o}, *C*H$_{sal}$), 163.98 (C^{m}, *C*H═N). The C^{tert} values were not given because of the small intensity of signals caused by an insufficient solubility of the product.

Complex VOL^2 (8). [8-(2′-Oxy-5′-phenylazo-phenyl)-3-methyl-1-phenyl-6-thiomethyl-1-one-4,5,7-triazaocta-1,3,5,7-tetraenato-(−)-2′-olato-(−)-*O*,*O*′,*N*4,*N*7]oxovanadium(IV): yield 0.43 g, 82%. Anal. Calcd for $C_{25}H_{21}N_5O_3SV$ (fw = 522.47): C, 57.47; H, 4.05; N, 13.40. Found: C, 57.26; H, 4.38; N, 13.02. UV ($CHCl_3$) λ_{max}, nm (ϵ, dm^3 mol^{-1} cm^{-1}): 476 (13 700), 441 (15 100), 360 (39 500), 315 (29 700), 243 (23 400). m/z = 522 (*I*, 100%).

Analyses and Physical Measurements. Elemental analyses were made by standard micromethods. Mass spectrometric analyses were performed on an Analytical VG 7070 EQ instrument using electron impact (EI) ionization. The ion source was operated under the following conditions: accelerating voltage, 9.4−9.6 kV; ionizing electron energy, 70 eV; ion source temperature, ∼180 °C. UV−vis spectra were obtained with a Lambda 6 Perkin-Elmer spectrophotometer. Both ^{1}H (400 MHz) and ^{13}C NMR (100 MHz) measurements were carried out on a Bruker Avance 400 spectrometer, using $CDCl_3$ and DMSO-d_6 as solvents. The assignments in the one-dimensional (1D) spectra were based on additional Dept, Hetcor, and correlation spectroscopy (COSY) experiments. Chloroform solution electron spin resonance (ESR) spectra were obtained with a Bruker spectrometer, type ER100D, using 2,2-diphenyl-1-picrylhydrazyl (DPPH) as the reference. All spectra were recorded at 298 and 170 K using a standard low-temperature apparatus Bruker ER 4111VT. Magnetic susceptibility of powdered samples was obtained at 290 K using Oxford instruments with a CF200 cryo-system and microbalance Cahn 2000. The equipment was previously calibrated with a $HgCo(NCS)_4$ standard.[29] Each magnetic measurement was corrected for cell and sample diamagnetic contributions.[30] Thermogravimetric analyses (TGA) were performed using a Mettler 4000 module. Samples were introduced in a closed aluminum oxide crucible and heated at a rate of 10 °C min^{-1} under nitrogen at atmospheric pressure. STAR^e software, version 8.10, was used to evaluate the data.

X-ray Analysis. Crystal data and details of data collection and refinement for compounds **2**, **3**, **4**, **7**, and **8** are given in Table 1. All crystals are characterized by a needle morphology, which in some cases made necessary the use of synchrotron radiation owing to their very small dimensions. Data collections for compounds **2**, **4**, and **7** were performed at the X-ray diffraction line XRD1 of the Elettra Synchrotron Light Laboratory (Trieste, Italy), using λ = 0.8, 0.7, and 0.7 Å, respectively. The programs MOSFLM,[31] version 6.11c, and SCALA[32] were used for data reduction. Intensity data for **3** and **8** were collected on a Bruker Apex CCD area detector using graphite monochromated Mo Kα radiation (λ = 0.710 73 Å). Data reduction was made using SAINT programs, and absorption corrections based on a multiscan were obtained by SADABS.[33] All structures were solved by direct methods using SIR92[34] and refined by SHELXL-97.[35] The program ORTEPIII was used for graphics.[36]

Second-Order NLO Response Measurements. The molecular quadratic hyperpolarizabilities (β_λ) were measured in a $CHCl_3$ solution by the solution-phase dc EFISH generation method,[37−39] which can provide direct information on the intrinsic molecular NLO properties through eq 1:

$$\gamma_{EFISH} = (\mu\beta_\lambda/5kT) + \gamma(-2\omega; \omega, \omega, 0) \quad (1)$$

where $\mu\beta_\lambda/5kT$ represents the dipolar orientational contribution and $\gamma(-2\omega; \omega, \omega, 0)$, a third-order term at frequency ω of the incident light, is the electronic contribution to γ_{EFISH} which is negligible for the kind of molecules investigated here. β_λ is the projection along the dipole moment axis of the vectorial component of the tensor of the quadratic hyperpolarizability, working with an incident wavelength λ. EFISH measurements were carried out with an incident wavelength of 1907 nm (chosen in order that its second harmonic, at 955 nm, occurs quite far from any significant absorption band of the investigated molecule, so that dispersive enhancements of the EFISH response are minimized[40]), at the Dipartimento di Chimica Inorganica Metallorganica e Analitica dell'Università di Milano, using a Q-switched, mode-locked Nd^{3+}:YAG laser. All experimental EFISH β_λ values are defined according to the "phenomenological" convention.[41]

Computational Details. The geometries of complexes **1**−**8** have been fully optimized within the DFT approach using the Becke's three-parameter hybrid exchange-correlation functional[42] with the nonlocal gradient correction of Lee, Yang, and Parr (B3LYP)[43] and the standard 6-31G** basis set. The unrestricted open-shell DFT method was adopted to treat the complexes of Cu and VO. Geometry optimizations were performed with the Gaussian98 package.[44]

The UV−vis spectra of **5**−**8** were calculated with the TDDFT formalism as implemented in the ADF package version 2005.01[45] using the geometries previously optimized by Gaussian98 and the BLYP exchange-correlation potential. Solvent effects were evalu-

(29) O'Connor, C. J.; Sinn, E.; Cukauskas, E. J.; Deaver, B. S., Jr. *Inorg. Chim. Acta* **1979**, *32*, 29−32.
(30) O'Connor, C. J. In *Progress in Inorganic Chemistry;* Lippard, S. J., Ed.; John Wiley & Sons: New York, 1982; Vol. 29, p 208.
(31) Leslie, A. G. W. Jnt CCP4/ESF-EACMB. *Newslett. Protein Crystallogr.* **1992**, 26.
(32) Evans, P. Jnt CCP4/ESF-EACMB. *Newslett. Protein Crystallogr.* **1997**, *33*, 22.
(33) *SMART*, *SAINT*, and *SADABS*; Bruker AXS Inc.: Madison, WI, U.S.A., 1997.
(34) Altomare, A.; Cascarano, G.; Giacovazzo, C.; Guagliardi, A.; Burla, M. C.; Polidori, G.; Camalli, M. *J. Appl. Crystallogr.* **1994**, *27*, 435.
(35) Sheldrick, G. M. *SHELXL97;* University of Göttingen: Göttingen, Germany, 1997.
(36) Burnett, M. N.; Johnson, C. K. *ORTEP-III: Oak Ridge Thermal Ellipsoid Plot Program for Crystal Structure Illustrations;* Oak Ridge National Laboratory Report ORNL-6895; National Technical Information Service, U.S. Department of Commerce: Springfield, VA, 1996.
(37) Levine, B. F.; Bethea, C. G. *Appl. Phys. Lett.* **1974**, *24*, 445−447.
(38) Singer, K. D.; Garito, A. F. *J. Chem. Phys.* **1981**, *75*, 3572−3580.
(39) Ledoux, I.; Zyss, J. *Chem. Phys.* **1982**, *73*, 203−213.
(40) Orr, B. J.; Ward, J. F. *Mol. Phys.* **1971**, *20*, 513−520.
(41) Willets, A.; Rice, J. E.; Burland, D. M.; Shelton, D. P. *J. Chem. Phys.* **1992**, *97*, 7590−7599.
(42) Becke, A. D. *J. Chem. Phys.* **1996**, *104*, 1040−1046.
(43) Lee, C.; Yang, W.; Parr, R. G. *Phys. Rev. B* **1988**, *37*, 785−789.
(44) Frisch, M. J.; Trucks, G. W.; Schlegel, H. B.; Scuseria, G. E.; Robb, M. A.; Cheeseman, J. R.; Zakrzewski, V. G.; Montgomery, J. A., Jr.; Stratmann, R. E.; Burant, J. C.; Dapprich, S.; Millam, J. M.; Daniels, A. D.; Kudin, K. N.; Strain, M. C.; Farkas, O.; Tomasi, J.; Barone, V.; Cossi, M.; Cammi, R.; Mennucci, B.; Pomelli, C.; Adamo, C.; Clifford, S.; Ochterski, J.; Petersson, G. A.; Ayala, P. Y.; Cui, Q.; Morokuma, K.; Malick, D. K.; Rabuck, A. D.; Raghavachari, K.; Foresman, J. B.; Cioslowski, J.; Ortiz, J. V.; Stefanov, B. B.; Liu, G.; Liashenko, A.; Piskorz, P.; Komaromi, I.; Gomperts, R.; Martin, R. L.; Fox, D. J.; Keith, T.; Al-Laham, M. A.; Peng, C. Y.; Nanayakkara, A.; Gonzalez, C.; Challacombe, M.; Gill, P. M. W.; Johnson, B. G.; Chen, W.; Wong, M. W.; Andres, J. L.; Head-Gordon, M.; Replogle, E. S.; Pople, J. A. *Gaussian 98*, revision A.11.3; Gaussian, Inc.: Pittsburgh, PA, 1998.

Table 1. Crystallographic and Data Collection Parameters for CuL^1 (**2**), $ZnL^1 \cdot CH_3OH$ (**3**), VOL^1 (**4**), $ZnL^2 \cdot CH_3OH$ (**7**), and VOL^2 (**8**)

	CuL^1 (**2**)	$ZnL^1 \cdot CH_3OH$ (**3**)	VOL^1 (**4**)	$ZnL^2 \cdot CH_3OH$ (**7**)	VOL^2 (**8**)
			Crystal Data		
empirical formula	$C_{19}H_{17}N_3O_2SCu$	$C_{20}H_{21}N_3O_3SZn$	$C_{19}H_{17}N_3O_3SV$	$C_{26}H_{25}N_5O_3SZn$	$C_{25}H_{21}N_5O_3SV$
moiety formula	$C_{19}H_{17}N_3O_2SCu$	$(C_{19}H_{17}N_3O_2SZn) \cdot CH_4O$	$C_{19}H_{17}N_3O_3SV$	$(C_{25}H_{21}N_5O_2SZn) \cdot CH_4O$	$C_{25}H_{21}N_5O_3SV$
M	414.96	448.83	418.36	552.94	522.47
crystal system	orthorhombic	triclinic	monoclinic	orthorhombic	monoclinic
space group	*Pbca*	$P\bar{1}$	$P2_1/n$	*Pbca*	$P2_1/c$
a, Å	9.312(3)	5.041(1)	10.165(18)	24.95(3)	9.099(2)
b, Å	18.545(17)	8.841(2)	16.575(7)	7.615(3)	14.423(3)
c, Å	20.892(12)	23.718(5)	11.10(2)	26.77(3)	18.446(4)
α, deg	90	87.17(3)	90	90	90
β, deg	90	86.79(3)	94.35(2)	90	92.03(3)
γ, deg	90	79.57(3)	90	90	90
V (Å^3), Z	3608(4), 8	1037.1(4), 2	1865(5), 4	5086(9), 8	2419.2(8), 4
radiation, λ (Å)	synchrotron, 0.8	Mo Kα, 0.710 73	synchrotron, 0.7	synchrotron, 0.7	Mo Kα, 0.710 73
detector	Mar345 Imaging plate	Bruker SMART APEX	MarCCD	MarCCD	Bruker SMART APEX
D_x, Mg m^{-3}	1.528	1.434	1.490	1.442	1.434
reflections for cell determination	76	1249	78	76	2351
2θ (deg) for cell determination	5.4−55.0	4.7−36.2	4.4−55.0	3.0−49.2	4.5−42.4
μ, mm^{-1}	1.345	1.310	0.669	1.086	0.534
temperature, K	293(2)	293(2)	293(2)	293(2)	293(2)
color, habit	red, needle	red, needle	red, needle	red, needle	red, prism
dimensions, mm	0.30 × 0.02 × 0.01	0.40 × 0.01 × 0.01	0.32 × 0.03 × 0.03	0.40 × 0.05 × 0.02	0.21 × 0.06 × 0.04
			Data Collection		
scan type	φ	φ and ω	φ	φ	φ and ω
$2\theta_{max}$ (deg)	55.0	55.0	55.0	49.2	55.0
h range	−10 → 10	−6 → 6	−13 → 13	−29 → 29	−11 → 11
k range	−21 → 21	−11 → 11	−21 → 21	−8 → 8	−18 → 18
l range	−24 → 24	−30 → 30	−13 → 13	−31 → 31	−23 → 23
intensity decay, %	none	2.40	none	none	none
measured reflections	19 016	14 113	17 497	26 261	33 671
independent reflections	2815	4779	4230	4005	5560
reflections with $I > 2\sigma(I)$	2391	2586	3764	3266	3247
R_{int}	0.031	0.096	0.030	0.060	0.089
			Refinement on F^2		
$R[F^2 > 2\sigma(F^2)]$, $wR[F^2 > 2\sigma(F^2)]$	0.0306, 0.0831	0.0594, 0.1310	0.0390, 0.1088	0.0672, 0.1737	0.0523, 0.1123
S	1.092	0.913	1.064	1.212	1.025
number of parameters	235	289	245	325	316
$(\Delta/\sigma)_{max}$	0.002	0.001	0.001	0.001	0.001
$\Delta\rho_{max}$, $\Delta\rho_{min}$ (e Å^{-3})	0.325, −0.343	0.394, −0.301	0.329, −0.430	0.598, −0.723	0.356, −0.247

ated through the conductor-like screening model (COSMO) as implemented in ADF[46] using the Bondi's van der Waals atomic radii to build the cavity around each atom. The introduction of solvent effects in the calculations determined a slight red shift (less than 10 nm) of the transitions with respect to the isolated molecule.

The TDDFT formalism was also used to compute the static and dynamic second harmonic generation (SHG, $\lambda = 1907$ nm) hyperpolarizability tensor β of Ni and Zn complexes **1**, **3**, **5**, and **7** (the ADF code for these calculations is currently restricted to closed-shell systems). In this case, the Van Leeuwen−Baerends (LB94) exchange-correlation potential,[47] which was shown to be appropriate for the calculation of NLO properties by virtue of its asymptotically correct behavior,[48] was used throughout. It is to be noted that the dipole moments of Zn complexes obtained with this functional were very similar (within 0.1 D) to those obtained with the B3LYP functional, while for Ni complexes the LB94 functional overestimated by almost 1 D the molecular dipoles. Hyperpolarizability calculations were performed on the isolated molecule to reduce the complexity of the calculation. Solvent effects, which were tested on complex ZnL^2 (**7**), were found to increase by 8 and 14% respectively the static and dynamic larger components (β_{xxx}) of the hyperpolarizability tensor. The quantity β_λ was obtained according to $\beta_\lambda = (\mu_x\beta_x + \mu_y\beta_y + \mu_z\beta_z)/\mu$, where $\beta_i = \beta_{iii} + (1/3)\sum_{j\neq i}(\beta_{ijj} + \beta_{iji} + \beta_{jii})$ are the components of β_{tot}, the vectorial part of tensor β.[49] The convention of tensor contraction when two indexes are equal is applied, for example, $\beta_{ikk} = \beta_{i11} + \beta_{i22} + \beta_{i33}$. The ADF β_{ijk} components of the hyperpolarizability tensor already converted to be compared with the experimental values have been used.[41] All ADF calculations were performed with the triple ζ doubly polarized Slater type orbital basis sets TZ2P for C, N, O, S, and H atoms and TZ2P+, including one diffuse function, for the metal atoms.

Results and Discussion

Synthesis and Characterization. The template condensation of 1-phenylbutane-1,3-dione mono-*S*-methylisothiosemicarbazone and salicylaldehyde or 5-phenylazo-salicylaldehyde in a basic medium (triethylamine) and in the presence of Ni(II), Cu(II), Zn(II), and VO(II) as matrixes yielded the complexes **1**−**8** in good yield and purity, according to Scheme 1. The synthesized compounds are crystalline brown

(45) te Velde, G.; Bickelhaupt, F. M.; van Gisbergen, S. J. A.; Fonseca Guerra, C.; Baerends, E. J.; Snijders, J. G.; Ziegler, T. *J. Comput. Chem.* **2001**, *22*, 931−967.
(46) Pye, C. C.; Ziegler, T. *Theor. Chem. Acc.* **1999**, *101*, 396−408.
(47) van Leeuwen, R.; Baerends, E. J. *Phys. Rev. A* **1994**, *49*, 2421−2431.
(48) van Gisbergen, S. J. A.; Snijders, J. G.; Baerends, E. J. *J. Chem. Phys.* **1998**, *109*, 10657−10668.
(49) Kanis, D. R.; Ratner, M. A.; Marks, T. J. *Chem. Rev.* **1994**, *94*, 195−242.

Table 2. Selected Experimental (when Available) and Computed Bond Lengths (Å) and Angles (deg) for Complexes **1**−**8**

	NiL^1 (**1**)	CuL^1 (**2**)		$ZnL^1 \cdot CH_3OH$ (**3**)		VOL^1 (**4**)		NiL^2 (**5**)	CuL^2 (**6**)	$ZnL^2 \cdot CH_3OH$ (**7**)		VOL^2 (**8**)	
	calcd	exptl	calcd	exptl	calcd	exptl	calcd	calcd	calcd	exptl	calcd	exptl	calcd
M−O1	*1.830*	1.912(2)	*1.899*	1.970(3)	*1.988*	1.934(3)	*1.959*	*1.828*	*1.895*	1.955(5)	*1.982*	1.936(2)	*1.955*
M−O2	*1.831*	1.906(2)	*1.888*	1.990(3)	*1.946*	1.933(2)	*1.951*	*1.835*	*1.894*	2.000(5)	*1.958*	1.950(2)	*1.961*
M−N1	*1.832*	1.923(2)	*1.914*	2.038(4)	*2.033*	2.032(2)	*2.049*	*1.830*	*1.912*	2.051(6)	*2.028*	2.021(2)	*2.045*
M−N3	*1.847*	1.947(2)	*1.950*	2.115(4)	*2.109*	2.049(2)	*2.086*	*1.848*	*1.951*	2.098(6)	*2.114*	2.048(2)	*2.087*
M−O3				2.066(3)	*2.158*	1.590(2)	*1.576*			2.062(5)	*2.150*	1.588(2)	*1.575*
O1−C5	*1.286*	1.298(3)	*1.285*	1.300(6)	*1.284*	1.304(3)	*1.292*	*1.287*	*1.286*	1.307(8)	*1.285*	1.299(3)	*1.293*
C5−C6	*1.402*	1.389(4)	*1.406*	1.388(7)	*1.407*	1.373(3)	*1.400*	*1.402*	*1.406*	1.375(10)	*1.407*	1.378(4)	*1.400*
C6−C7	*1.401*	1.410(4)	*1.405*	1.420(7)	*1.413*	1.410(3)	*1.408*	*1.401*	*1.405*	1.413(9)	*1.412*	1.401(4)	*1.408*
C7−N1	*1.337*	1.321(3)	*1.334*	1.323(6)	*1.331*	1.322(3)	*1.336*	*1.338*	*1.335*	1.315(8)	*1.332*	1.321(4)	*1.336*
N1−N2	*1.380*	1.388(3)	*1.378*	1.400(5)	*1.379*	1.404(3)	*1.386*	*1.380*	*1.377*	1.387(7)	*1.378*	1.403(3)	*1.385*
N2−C1	*1.293*	1.292(3)	*1.297*	1.300(6)	*1.300*	1.291(3)	*1.293*	*1.293*	*1.297*	1.295(8)	*1.299*	1.288(4)	*1.293*
C1−S	*1.778*	1.757(3)	*1.784*	1.757(5)	*1.793*	1.745(3)	*1.780*	*1.777*	*1.783*	1.743(7)	*1.791*	1.749(3)	*1.779*
C1−N3	*1.398*	1.397(3)	*1.391*	1.396(6)	*1.383*	1.403(3)	*1.399*	*1.400*	*1.393*	1.398(8)	*1.385*	1.415(4)	*1.400*
N3−C2	*1.322*	1.310(3)	*1.317*	1.294(5)	*1.311*	1.310(3)	*1.317*	*1.320*	*1.315*	1.291(8)	*1.309*	1.310(4)	*1.316*
C2−C3	*1.408*	1.416(4)	*1.413*	1.437(6)	*1.421*	1.410(3)	*1.416*	*1.411*	*1.416*	1.432(9)	*1.424*	1.423(4)	*1.418*
C3−C4	*1.443*	1.435(4)	*1.449*	1.432(6)	*1.449*	1.423(3)	*1.443*	*1.445*	*1.451*	1.419(9)	*1.451*	1.425(4)	*1.445*
C4−O2	*1.292*	1.306(3)	*1.291*	1.316(5)	*1.294*	1.306(3)	*1.299*	*1.287*	*1.286*	1.288(8)	*1.287*	1.295(3)	*1.294*
O1−M−N1	*94.6*	93.6(1)	*93.4*	91.5(2)	*89.6*	87.1(1)	*86.4*	*94.7*	*93.5*	91.5(2)	*90.0*	87.6(1)	*86.5*
O1−M−N3	*178.5*	174.2(1)	*175.0*	162.3(1)	*153.0*	145.9(1)	*143.5*	*178.8*	*175.1*	162.5(2)	*153.2*	144.9(1)	*143.0*
O1−M−O2	*86.5*	91.3(1)	*91.7*	98.9(1)	*98.1*	88.5(1)	*88.8*	*86.5*	*91.6*	97.8(2)	*97.6*	89.4(1)	*88.7*
N1−M−N3	*84.0*	81.0(1)	*81.8*	76.1(2)	*76.8*	75.8(1)	*75.4*	*84.1*	*81.9*	76.3(2)	*76.9*	76.2(1)	*75.5*
N1−M−O2	*178.7*	174.2(1)	*174.6*	152.4(2)	*160.7*	140.9(1)	*140.8*	*178.8*	*174.7*	151.9(2)	*159.5*	145.7(1)	*141.4*
N3−M−O2	*94.8*	94.2(1)	*93.2*	87.3(1)	*88.7*	86.8(1)	*86.0*	*94.8*	*93.0*	87.9(2)	*88.3*	87.1(1)	*86.1*

products, soluble in chloroform, acetone, methanol, and dimethylsulfoxide. They were obtained with excellent yield because of the intramolecular hydrogen bond between the fairly acidic phenolic hydrogen and the carbonyl oxygen atom in salicylaldehyde or its derivative, which catalyzes the condensation with benzoylacetone-*S*-methylisothiosemicarbazone. The coordination to the 3d metal ions of the quadridentate (ONNO) ligand is realized by means of nitrogen atoms N^1 and N^4 of the isothiosemicarbazide fragment and two oxygen atoms of the benzoylacetonic and salicylidene fragments. Composition and identity of the assembled systems were deduced from elemental analysis and IR, UV−vis, NMR, and mass spectra. The distinctive feature of the mass spectra of compounds **1**−**8** is the presence of peaks of molecular ions $[M]^+$ with 100% intensity and doubly charged ions $[M]^{2+}$, both indicating a large stability of these complexes toward EI. Compounds **1**−**8** exhibit excellent thermal stability, comparable to that reported for bis(salicylaldiminato)Ni complexes[5] (see TGA curves in Supporting Information, Figure S1). Decomposition temperatures were 270, 280, 310, and 260 °C for NiL^1, CuL^1, ZnL^1, and VOL^1, respectively, and 295, 300, 240, and 300 °C for NiL^2, CuL^2, ZnL^2, and VOL^2, respectively.

The ^1H and ^{13}C NMR data for nickel and zinc complexes are reported in Experimental Section with atom labeling in Scheme 2. The presence of the iminic proton H^m between 7.96 and 8.77 ppm confirms the assembling of tetradentate Schiff base ligands. In general, all proton signals of the complexes bearing the diazophenyl group in para position to the salicylaldehyde unit appear at lower field than their analogues **1** and **3**. This effect is more evident for the resonance of the azomethine Schiff base bond CH═N for the Zn species, which appears at 8.56 ppm for **3** and 8.77 ppm for **7**. In the ^{13}C NMR data, the same tendency was depicted for the C^mH═N azomethyne carbon whose signal is shifted at lower field in the diazophenyl analogues (by 0.64 and 0.37 ppm for Ni and Zn complexes, respectively).

A comparison between the NMR spectra of **1** and those of the closely related compound bearing *o*-aminobenzaldehyde instead of the *o*-hydroxybenzaldehyde unit[19] indicates that practically all of the carbon resonances of the latter are shifted to upfield (by 0.17−0.48 ppm) with respect to the former compound. The most evident effect is observed for the azomethyne carbon C^mH═N, whose value is 155.30 ppm for **1** and 146.98 ppm for the same atom in the compound of ref 19. A significant shift (7 ppm) is also observed for the tertiary carbon atoms $C^{k,g}$ as well as for the substituted benzaldehyde ring $C^{o,r,n,p,q}$ (2−3 ppm shift to stronger field). The ^1H resonances are slightly shifted both downfield (for Me groups, H^f and H^m) and upfield (for benzaldehyde protons, $H^{r,q,p,o}$). All spectral data are consistent with the given structure.

Both copper compounds CuL^1 (**2**) and CuL^2 (**6**) are paramagnetic with effective magnetic moments (at 290 K) 1.9 and 2.0 μ_B, respectively, which are slightly above the spin-only magnetic moment value 1.73 μ_B for the d^9 configuration ($S = 1/2$),[50,51] very near to the values in the range 1.80−1.95 μ_B, consistent with the expected monomeric structure of the complexes. The ESR spectra at room temperature exhibit an asymmetric quadruplet with $g = 2.096$ for **2** and $g = 2.095$ for **6**, with average values of $A = 90$ G (**2**) and 88 G (**6**) and $\Delta H_{pp} = 45$ G (**2**) and 48 G (**6**). One may note some badly resolved hyperfine lines in the ESR spectra because of the interaction with the N nuclei. At low temperature (120 K), the signals of **6** are badly resolved as a result of the overlapping of *g* parallel and *g* perpendicular signals. ESR spectrum of **2** at 170 K shows two quadruplets with $g^{\parallel} = 2.29$ G and $A^{\parallel} = 137$ G, $g^{\perp} = 2.12$ G and $A^{\perp} = 23$ G.

Oxovanadium(IV) complexes (**4** and **8**) have, at room temperature (290 K), effective magnetic moments equal to

(50) Cotton, F. A.; Wilkinson, G. *Advanced Inorganic Chemistry*, 5th ed.; Wiley−Interscience: New York, 1988; p 768.
(51) McConnell, H. M. *J. Chem. Phys.* **1956**, *25*, 709−711.

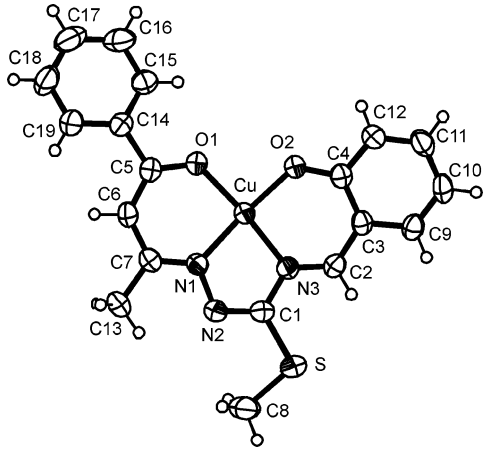

Figure 1. ORTEP of **2** with an atom-numbering scheme. Displacement ellipsoids are drawn at the 50% probability.

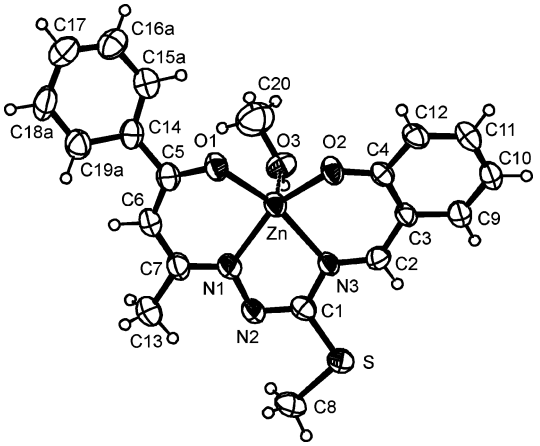

Figure 2. ORTEP of **3** with an atom-numbering scheme. Displacement ellipsoids are drawn at the 40% probability.

1.7 and 1.8 μ_B, respectively, which are in good agreement with the predicted spin-only value of 1.73 μ_B for d^1-vanadium(IV).[52] The ESR spectrum at room temperature exhibits an asymmetric octuplet, without hyperfine lines, with $g = 1.998$ and 1.988 (for **4** and **8**, respectively), and average values of $A = 97$ G (**4**) and 96 G (**8**) and $\Delta H_{pp} = 16$ G (**4**) and 17 G (**8**). The eight lines in the electron paramagnetic resonance (EPR) spectrum of VO compounds are due to the hyperfine coupling of an unpaired electron to the vanadium nuclear spin (^{51}V with nuclear spin number $I = 7/2$) which corresponds to the presence of a single vanadium atom in the molecule. At room temperature, the anisotropy is not detected because of the rapid tumbling of the molecule. At low temperature (120 K), the signals for **8** are badly resolved, with two octuplets. The ESR spectrum of **4** at 170 K displays well-resolved axial anisotropy with two sets of eight line patterns. Spin Hamiltonian parameters $g^{\|} = 1.96$ G and $A^{\|} = 170$ G, $g^{\perp} = 1.97$ G and $A^{\perp} = 63$ G are as expected for square pyramidal oxovanadium(II) complexes.

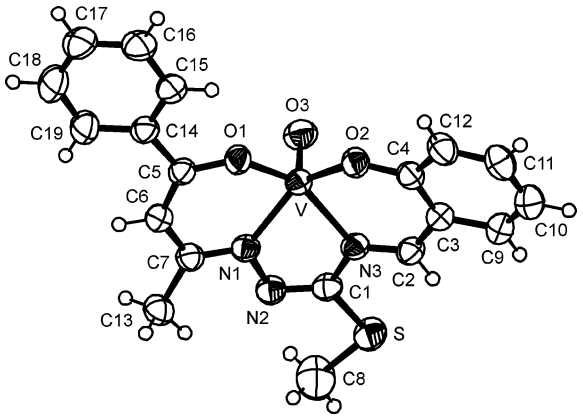

Figure 3. ORTEP of **4** with an atom-numbering scheme. Displacement ellipsoids are drawn at the 50% probability.

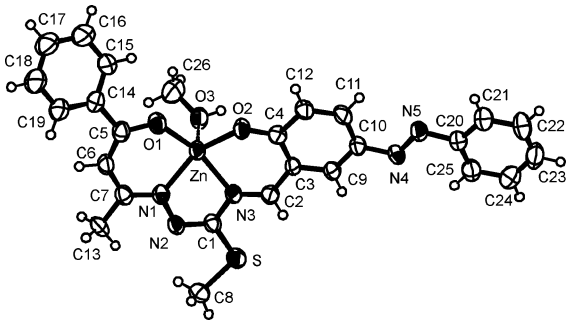

Figure 4. ORTEP of **7** with an atom-numbering scheme. Displacemen-tellipsoids are drawn at the 50% probability.

X-ray Diffraction Studies. Selected bond distances and angles of molecules **2**, **3**, **4**, **7**, and **8** are reported in Table 2, and perspective views, along with the atom numbering scheme, are shown in Figures 1−5.

The structure of the CuL^1 complex (**2**) shows the expected square-planar four-coordinate environment around the Cu center, with very slight tetrahedral distortion from planarity (see Table 3). The Cu atom is placed approximately at the center of the tetrahedron, and the N atoms are symmetrically placed farther from the $[N_2O_2]$ least-squares (l.s.) plane with respect to the O atoms.

X-ray analysis of complexes ZnL^1 (**3**) and ZnL^2 (**7**) reveals the presence of one methanol molecule in the metal coordination sphere. The geometry around the Zn(II) center can be described as a distorted square pyramid where the oxygen atom of the methanol molecule (O3) occupies the apical position, the atoms O1, N1, N3, and O2 define the basal plane, and the metal atom is placed at 0.3366 Å (ZnL^1) and 0.348 Å (ZnL^2) from this plane. The Zn−O3 bond is almost orthogonal to the $[N_2O_2]$ basal plane, as indicated by the angle formed with the normal to this plane, 1.8(1)° and 2.4(2)° in ZnL^1 and ZnL^2, respectively. The atoms of the basal plane are subjected to a greater tetrahedral deviation from planarity with respect to the CuL^1 complex (see Table 3).

Square pyramid coordination geometry is observed also in complexes VOL^1 (**4**) and VOL^2 (**8**), where the V−O3 bond forms angles equal to 0.71(7)° and 1.35(9)° in VOL^1 and VOL^2, respectively, with the normal to the $[N_2O_2]$ l.s. plane. It is to be noted that, in the two structures, the V−O3 bond points in opposite directions. Unlike the Zn complexes, the basal plane of VOL^1 and VOL^2 presents only a slight tetrahedral distortion, very similar to (in VOL^1) or also lower

(52) Collison, D.; Gahar, B.; Garner, C. D.; Mabbs, F. E. *J. Chem. Soc., Dalton Trans.* **1980**, 667.

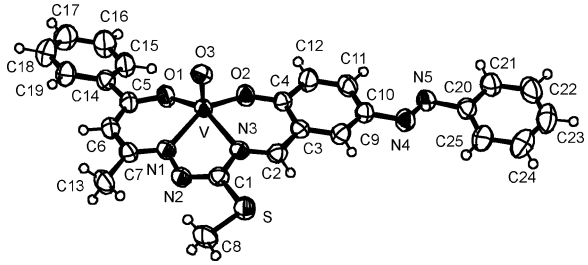

Figure 5. ORTEP of **8** with an atom-numbering scheme. Displacement ellipsoids are drawn at the 50% probability.

Table 3. Experimental Atom Deviations (Å) from the Best Basal Plane in **2**, **3**, **4**, **7**, and **8**[a]

atom	CuL^1 (**2**)	$ZnL^1 \cdot CH_3OH$ (**3**)	VOL^1 (**4**)	$ZnL^2 \cdot CH_3OH$ (**7**)	VOL^2 (**8**)
O1	−0.036(2)	0.060(3)	0.035(2)	−0.067(5)	0.008(2)
N1	0.050(2)	−0.103(4)	−0.044(2)	0.099(6)	−0.011(2)
N3	−0.049(2)	0.080(4)	0.044(2)	−0.105(6)	0.011(2)
O2	0.036(2)	−0.054(3)	−0.035(2)	0.073(5)	−0.008(2)
M	−0.0081(5)	0.3366(8)	0.611(1)	−0.348(1)	−0.5799(6)

[a] Metal center M is excluded from the definition of the l.s. planes.

than (in VOL^2) that observed in the Cu complex. Moreover, the V atom is considerably pushed out from the basal plane toward the O3 atom.

When comparing complexes of different coordination metals with the same ligand L^1, we note a significant expansion of the central core upon going from Cu to VO and then to Zn. This is particularly evident by looking at the M−N bond distances. On average, the M−O bond lengthening with respect to the Cu complex is 0.025 and 0.070 Å in VOL^1 and ZnL^1, respectively, and the M−N bond lengthening is 0.106 and 0.142 Å in VOL^1 and ZnL^1, respectively. On the other hand, a comparison between complexes of the same metal (Zn or VO) with different ligands (L^1 and L^2) does not reveal significant differences in the coordination geometry. The only detectable effect (confirmed by theoretical calculations, see below) is a small lengthening of the M−O2 bonds upon going from L^1 to L^2 (+0.010 and +0.017 Å for Zn and VO complexes, respectively) because of a shortening of the O2−C4 bonds in para position with respect to the phenylazo substituent (−0.028 and −0.011 Å for Zn and VO complexes, respectively).

In Table 2, the bond lengths of the three chelate rings are also reported. Within the experimental error, they are very similar in all complexes, independent of the metal center or of the ligand. On the whole, they are indicative of substantial π delocalization of the electron density through these rings.

Analysis of the crystal packing of complexes **2**, **3**, **4**, **7**, and **8** reveals in all cases the formation of stacked structures with metal···ligand intermolecular interactions. The separation between molecules along the stack can be indicative of the relative strength of such interactions in the crystal. To this aim, we have computed the distances between [N_2O_2] l.s. planes in all structures. In CuL^1, where infinite chains are formed along the stack, the interplanar distance is 3.29(1) Å, and the shortest interatomic contacts are $Cu\cdots C3_{1/2+x,y,3/2-z}$, 3.208(3) Å and $Cu\cdots C6_{-1/2+x,y,3/2-z}$, 3.195(3) Å. Infinite chains are also observed in both Zn complexes, where the interplanar distances are 3.43(1) and 3.37(2) Å in ZnL^1 and ZnL^2, respectively. In this case, adjacent molecules along the stack are also joined together by relatively strong O3−H3···O2 hydrogen bonds (H···O = 1.81 and 1.84 Å; O−H···O = 167 and 165° in ZnL^1 and ZnL^2, respectively). Dimeric structures are observed in both VO complexes, where the molecules of a dimer are oriented with the VO bonds pointing inward. The interplanar separations are 3.27(1) and 3.31(1) Å (within the dimer) and 3.56(1) and 3.45(1) Å (between adjacent dimers) in VOL^1 and VOL^2, respectively. The different packing of the complexes, together with their different degree of planarity, can explain the observed variations in the tilting angle of the phenyl ring around the C5−C14 bond. It assumes the lowest value in CuL^1, 14.66(8)°, and significantly larger values in the other complexes [23.9(2), 24.49(6), and 30.63(9)° in ZnL^2, VOL^1, and VOL^2, respectively]. In ZnL^1, the phenyl ring is disordered over two alternative and equiprobable positions A and B, which are tilted around the C5−C14 bond by 21.6(3) and 43.3(3)°, respectively. In Figure 2, only conformation A is shown.

Between nearest neighbor molecules of different stacks, only very weak interactions are observed, which can account for the needle morphology of the crystals.

DFT Computed Structures and Dipole Moments. Structures of complexes **1**−**8** were fully optimized at the all-electron B3LYP/6-31G** level, starting from the experimental X-ray geometries when available (see details in Experimental Section). According to the results of the magnetic measurements (see above), Cu and VO complexes were optimized in their doublet spin state.

Some relevant geometrical parameters are reported in Table 2 together with the corresponding experimental values available. Comparison between optimized and experimental geometries indicates very good agreement in the case of CuL^1 while, for the Zn and VO complexes, the metal−ligand distances are reproduced approximately within 0.04 Å. Moreover, the oxygen atom of the coordinated methanol molecule in Zn complexes is predicted to be farther than 0.09 Å from the metal atom with respect to the X-ray structure. This larger discrepancy can also be ascribed to neglecting packing forces in the calculations.

Apart from these differences, which anyway are of the same order of magnitude by which experimental metal−ligand bond lengths are generally reproduced by gradient-corrected DFT methods,[53] the trend obtained at the theoretical level for the complexes with different ligands and coordination metals is the same as that experimentally observed; that is, the dimensions of the central core are found to increase in the order Ni(II) < Cu(II) < VO(II) < Zn(II). Moreover, upon going from L^1 to L^2, a small but systematic increase of the M−O2 bond length with concomitant decrease of the C4−O2 bond length is observed, the larger variations (+0.012 and −0.007, respectively) being found in Zn complexes.

The dipole moments μ of the B3LYP/6-31G** optimized complexes **1**−**8** are reported in Table 4. Because in all of

(53) Koch, W.; Holthausen, M. C. *A Chemist's Guide to Density Functional Theory*, 2nd ed.; Wiley: New York, 2000.

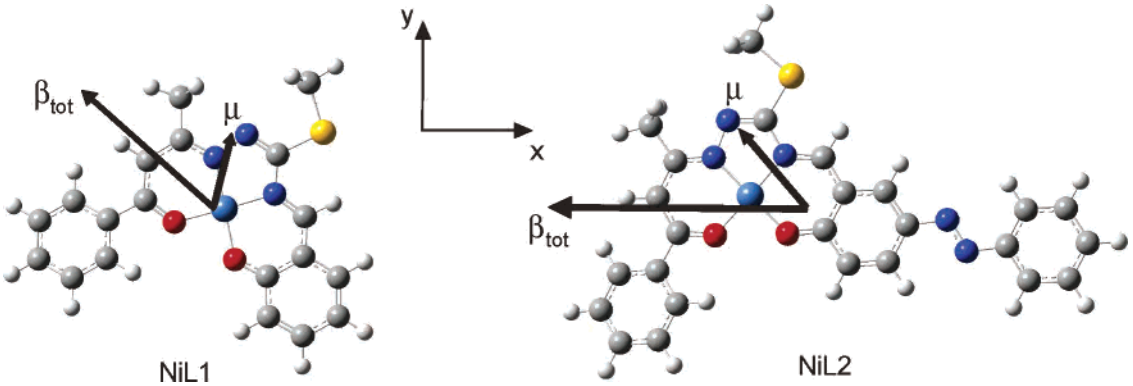

Figure 6. Optimized B3LYP/6-31G** structures of NiL^1 and NiL^2 with an axes reference system and computed molecular dipoles and hyperpolarizabilities (arbitrary units for μ and β_{tot} vectors).

Table 4. Computed B3LYP/6-31G** and Experimental (if Available) Dipole Moments for Complexes **1**−**8**[a]

compound	μ_x	μ_y	μ_z	μ	μ_{expt}[b]
NiL^1	1.050	2.241	0.109	2.473	
CuL^1	0.950	2.332	0.105	2.520	
ZnL^1	−0.801	1.699	2.940	3.489	3.9
VOL^1	1.128	2.089	−3.341	4.098	
NiL^2	−2.243	2.673	0.104	3.491	2.4
CuL^2	−2.176	2.751	0.042	3.508	2.3
ZnL^2	−4.024	1.643	2.896	5.222	5.9
VOL^2	−1.178	2.457	3.437	4.386	2.4

[a] μ in debye. [b] Solvent is $CHCl_3$; experimental standard uncertainty is estimated as ±1 D.

the investigated systems it is not possible to identify a particular molecular axis along which charge distribution is principally polarized, we report in Table 4 the vector components of μ along the three Cartesian directions, according to the standard orientation of the Gaussian program, where the *z* axis of the coordinated system is approximately normal to the $[N_2O_2]$ plane, the *x* axis lies in the direction of the largest extension of the molecule, and the *y* axis completes the right-handed reference system (see two representative examples in Figure 6). Our calculations reproduced, within the experimental uncertainty, the measured values (obtained by the Guggenheim method[54]), also reported in Table 4, with the only exception of VOL^2. In the latter case, the experimental value could be affected by the presence of water molecules hydrogen bonded to the oxygen atom of the vanadyl group and/or coordinated to the vanadium atom in such a way to reduce the μ_z component.

The values of μ for this class of compounds are quite small, in particular, if compared with those of unsubstituted [M(salen)] and [M(salophen)] complexes, which amount to about 6−8 D depending on the metal (Ni, Cu, or Co) and the method (experimental or theoretical) used for their determination.[24−26] Some considerations are however noteworthy. The *z* component is clearly negligible in the planar Ni and Cu complexes, while it is significant in the square pyramidal Zn and VO complexes (note the opposite sign of μ_z in VOL^1 and VOL^2 because of the different orientation of the V=O bonds in the two molecules according to the experimental structures). However, on account of the NLO properties of these complexes (see below), the more important directions of polarization lie in the *xy* plane. The *y* component is principally due to the asymmetric $[N_2O_2]$ coordination around the metal atom, similar to what was found in unsubstituted [M(salen)] and [M(salophen)] complexes,[24−26] but it is significantly lower than that of the latter compounds. This component is found to slightly decrease in the order Cu > Ni > Zn > VO and remains essentially unvaried upon passing from the L^1 to the L^2 ligand. On the other hand, the *x* component clearly depends on the ligand, undergoing an inversion of direction for Ni, Cu, and VO complexes and an increase in magnitude upon going from L^1 to L^2. In ML^2 complexes, this component is directed from the phenylazo-salicylaldehyde toward the butane-dione moiety (see Figure 6), and its magnitude is found to decrease in the order Zn > Ni ∼ Cu > VO. A comparison of the μ_x values of ML^2 complexes with that of the [Cu(salen)] complex carrying the NO_2 group in position 5, amounting to about 8 D,[26] indicates that the phenylazo group acts as a much weaker electron acceptor with respect to NO_2. Finally, it is to be noted that the relatively large *x* component of Zn complexes is due to the coordinated methanol molecules, which during geometry optimization rotates with respect to the experimental geometry and reorients so as to increase the total dipole moment. Geometry optimizations of ZnL^1 and ZnL^2 without methanol lead in fact to μ_x values comparable to those of Ni and Cu complexes (2.26 and 3.32 D, respectively).[55]

Electronic Absorption Spectra. The UV−vis spectra of complexes **1**−**8** in chloroform are reported in Table 5 and, only for **5**−**8**, in Figure 7. They show essentially three sets of common bands, falling in the ranges 296−315, 360−386, and 475−495 nm. In some cases, a fourth band appears in the range 419−448 nm. The position of the signals is dependent on the metal atom but scarcely dependent on the ligand (only the intermediate band of VO complexes undergoes a significant blue shift from 386 to 360 nm on going from L^1 to L^2 ligand). On the other hand, the intensity

(54) (a) Guggenheim, E. A. *Trans. Faraday Soc.* **1949**, *45*, 714−720. (b) Smith, W. *Electric Dipole Moments;* Butterworth Scientific Publications: London, 1965. (c) Thompson, B. H. *J. Chem. Educ.* **1966**, *43*, 66−73. Solubility problems hampered the measurements of some compounds.

(55) In this case, a planar, slightly distorted coordination geometry around the Zn atom was obtained, closely resembling that of Ni and Cu complexes.

Table 5. Electronic Spectral Data λ_{max} (ϵ) for Complexes **1**−**8** in $CHCl_3$[a]

NiL^1	CuL^1	ZnL^1	VOL^1	NiL^2	CuL^2	ZnL^2	VOL^2
296 (19500)	311 (25000)	300 (18000)	313 (17100)	294 (20400)	310 (23300)	304 (27300)	315 (29700)
346 (13800)							
372 (11900)	360 (16800)	368 (15200)	386 (17300)	375 (34000)	360 (34800)	360 (34600)	360 (39500)
	435 (18300)	419 (10600)	424sh (12200)		448 (14200)		441 (15100)
485(10100)		489 (10900)	475sh (9400)	495 (13100)	490 (12800)	479 (13900)	476sh (13700)

[a] λ_{max} in nanometers; ϵ in $dm^3\ mol^{-1}\ cm^{-1}$.

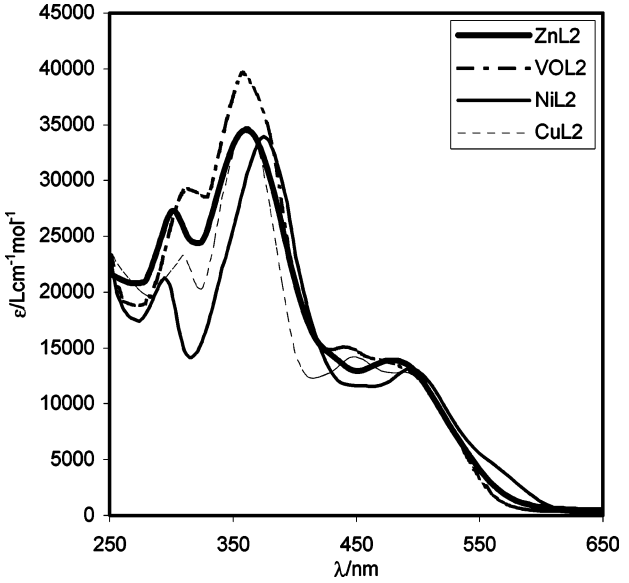

Figure 7. Experimental UV−vis spectra of complexes NiL^2, CuL^2, ZnL^2, and VOL^2 in $CHCl_3$.

of the bands is strongly dependent on the ligand, in particular, as the central bands (360−386 nm) are concerned. The maximum variation is observed in Ni complexes; the band at 360−370 nm increases from log $\epsilon = 4.08$ (for NiL^1) to 4.53 (for NiL^2). The phenylazo group therefore appears to exert a strong hyperchromic effect on complexes **5**−**8**. This intensity increase can be ascribed to an increase of the transition dipole moments, indicating that the excited states involved in the transitions are characterized by large dipole moments, unlike the ground state. It is then presumable that the central bands, where this effect is particularly pronounced, are the principal charge-transfer bands responsible for the NLO response of these complexes.

In order to interpret the optical spectra of the examined compounds, theoretical TDDFT calculations have been performed on complexes with the L^2 ligand in chloroform. The properties of the more significant transitions are reported in Table 6. Their positions are in all cases shifted toward lower energies with respect to the experimental ones. This downshift appears to be typical of the LB94 exchange-correlation functional[56] and, in general, of non-hybrid functionals.[57] The use of hybrid functionals in TDDFT calculations may allow not only for the recovery of this underestimation, leading to very good agreement with experiment in some cases,[58] where the B3LYP functional has been used, but also for a strong overestimation of the excitation energies, as found using B3P86.[59] Apart from the lack of quantitative agreement between computed and experimental transitions, our simulated spectra coincide with the experimental ones as the number of major bands is concerned, that is, three bands for the closed-shell complexes and four bands for the open-shell ones. Moreover, almost all transitions of the computed spectra and, in particular, the central ones are characterized by large values of the transition dipole moments μ_{eg}, which confirms that the excited states are characterized by large dipole moments. This is especially evident for ZnL^2 and VOL^2 complexes.

By analyzing the principal MO → MO contributions to the transitions, we can appreciate the different role played by the metal atoms in determining the electronic spectrum of the complexes. In all cases, the d orbitals of the metal are involved in one or more transitions which are, in particular, metal-to-ligand charge-transfer (MLCT) transitions for the closed-shell Ni and Zn complexes and ligand-to-metal charge-transfer (LMCT) transitions for the open-shell Cu and VO complexes. Moreover, the metal atom is significantly involved in NiL^2 and CuL^2 and only marginally involved in ZnL^2 and VOL^2. Importantly, most transitions, independent of their nature (MLCT, LMCT, or intra-ligand $\pi \rightarrow \pi^*$), are characterized by charge transfer toward the phenylazo-salicylaldehyde moiety or some portions of it (in particular the N═N bond). This indicates a well-defined direction of polarization for the most important low-lying excited states.

Investigation of Second-Order NLO Properties. The values of $\mu\beta_\lambda$ for the title complexes as obtained by EFISH measurements and only for closed-shell systems by theoretical calculations are reported in Tables 7 and 8, respectively. The corresponding experimental and theoretical β_λ values were obtained by using respectively the experimental and the computed dipole moments. By analyzing the experimental results, we observe large $\mu\beta_\lambda$ and β_λ magnitudes for complexes CuL^2 and ZnL^2, similar to those reported for the more promising bis(salicylaldiminato)metal complexes.[3,5,23] For comparison, the azo dye Disperse Red 1 (4-[*N*-ethyl-*N*-(2-hydroxyethyl)]amino-4′-nitroazobenzene) currently used as a dopant molecule in polymer matrices for electro-optic

(56) van Gisbergen, S. J. A.; Groeneveld, J. A.; Rosa, A.; Snijders, J. G.; Baerends, E. J. *J. Phys. Chem. A* **1999**, *103*, 6835−6844.
(57) Fantacci, S.; De Angelis, F.; Selloni, A. *J. Am. Chem. Soc.* **2003**, *125*, 4381−4387.
(58) (a) De Angelis, F.; Fantacci, S.; Selloni, A. *Chem. Phys. Lett.* **2004**, *389*, 204−208. (b) De Angelis, F.; Fantacci, S.; Selloni, A.; Nazeeruddin, M. K. *Chem. Phys. Lett.* **2005**, *415*, 115−120.
(59) (a) Coe, B. J.; Jones, L. A.; Harris, J. A.; Brunschwig, B. S.; Asselberghs, I.; Clays, K.; Persoons, A.; Garin, J.; Orduna, J. *J. Am. Chem. Soc.* **2004**, *126*, 3880−3891. (b) Coe, B. J.; Harris, J. A.; Jones, L. A.; Brunschwig, B. S.; Song, K.; Clays, K.; Garin, J.; Orduna, J.; Coles, S. J.; Hursthouse, M. B. *J. Am. Chem. Soc.* **2005**, *127*, 4845−4859.

Table 6. Principal[a] Computed Electronic Transitions (λ) of Complexes **5**−**8** in $CHCl_3$, along with the Associated Oscillator Strengths (f), the Transition Dipole Moments (μ_{eg}), and the More Important Contributions to the Transition

	NiL^2	CuL^2	ZnL^2	VOL^2
λ (nm)	398	350	331	343
f	0.349	0.225	0.183	0.141
μ_{eg} (D)	5.43	4.09	3.58	3.21
contributions (weight)	$d_{xz} \rightarrow \pi^*_{N=N}$ (0.36) $p_z(S) \rightarrow \pi^*_{sal}$ (0.23) $p_z(S) \rightarrow \pi^*_{N=N}$ (0.15)	$\pi_{delocalized} \rightarrow \pi^*_{N=N}$ (0.24)[b] $\pi_{delocalized} \rightarrow \pi^*_{sal}$ (0.14)[b]	$p_z(S) \rightarrow \pi^*_{butanedione}$ (0.29) $\pi_{sal} \rightarrow \pi^*_{sal-phenylazo}$(0.21)	$p_z(S) \rightarrow \pi^*_{butanedione}$ (0.39)[b] $\pi_{delocalized} \rightarrow \pi^*_{sal}$ (0.24)[b]
λ (nm)	476	430	428	420
f	0.331	0.226	0.752	0.708
μ_{eg} (D)	5.79	4.55	8.27	7.95
contributions (weight)	$d_{yz} \rightarrow \pi^*_{N=N}$ (0.35) $d_{yz} \rightarrow \pi^*_{sal}$ (0.26) $d_{xz} \rightarrow \pi^*_{phenyl-butanedione}$ (0.15)	$\pi_{sal-phenylazo} \rightarrow \pi^*_{N=N}$ (0.29)[b] $\pi_{phenyl(sal)} \rightarrow d_{xy}$ (0.24)[c] $\pi_{phenyl(butanedione)} \rightarrow d_{xy}$ (0.11)[c]	$\pi_{sal} \rightarrow \pi^*_{N=N}$ (0.47) $\sigma_{Zn-ligand} \rightarrow \pi^*_{N=N}$ (0.27)	$\pi_{sal-phenylazo} \rightarrow \pi^*_{N=N}$ (0.59)[b] $p_z(S) \rightarrow \pi^*_{sal}$ (0.20)[b]
λ (nm)		456[d]		446
f		0.313		0.144
μ_{eg} (D)		5.51		3.70
contributions (weight)		$\sigma_{Cu-ligand} \rightarrow d_{xy}$ (0.41)[c] $\pi_{Cu-ligand} \rightarrow d_{xy}$ (0.22)[c] $p_z(S) \rightarrow d_{xy}$ (0.17)[c]		$\pi_{butanedione-thsc} \rightarrow \pi^*_{butanedione}$ (0.40)[b] $\pi_{butanedione-thsc} \rightarrow d_{x2-y2}$ (0.25)[c]
λ (nm)	545	603	595	612
f	0.230	0.156	0.319	0.161
μ_{eg} (D)	5.16	4.47	6.35	4.58
contributions (weight)	$\pi_{delocalized} \rightarrow \pi^*_{sal}$ (0.76) $d_{yz} \rightarrow \pi^*_{N=N}$ (0.12)	$\pi_{butanedione-thsc} \rightarrow \pi^*_{sal}$ (0.71)[b] $\pi_{butanedione-thsc} \rightarrow \pi^*_{N=N}$ (0.16)[b]	$\pi_{butanedione-thsc} \rightarrow \pi^*_{sal-phenylazo}$ (0.75)	$\pi_{butanedione-thsc} \rightarrow \pi^*_{sal}$ (0.86)[b]

[a] Only transitions with $f > 0.1$ are included. [b] Contribution from both α and β electrons. [c] Contribution from only the β electron. [d] In this region of the spectrum, another transition was found (λ = 449 nm, f = 0.256, μ_{eg} = 4.18 D) whose principal contribution is $\pi_{Cu-ligand}(\beta) \rightarrow d_{xy}(\beta)$ (weight = 0.73).

Table 7. Experimental EFISH First Hyperpolarizabilities of Complexes **3** and **5**−**8**[a]

compound	$\mu\beta_\lambda$	β_λ[b]	compound	$\mu\beta_\lambda$	β_λ[b]
ZnL^1	−340	−87	ZnL^2	−1650	−280
NiL^2	−176	−73	VOL^2	−200	−83
CuL^2	−538	−234			

[a] Hyperpolarizabilities are given in 10^{-30} esu, and the $\mu\beta_\lambda$ product is given in 10^{-48} esu. The experimental errors associated with $\mu\beta_\lambda$ are about ±10−15%. [b] Evaluated using the experimental dipole moments (see Table 4).

Table 8. Theoretical First Hyperpolarizabilities of Complexes **1**, **3**, **5**, and **7**[a]

	NiL^1	ZnL^1	NiL^2	ZnL^2
		$\lambda = 1.907\ \mu$m		
$\mu\beta_\lambda$[b]	22.22	87.60	261.63	584.59
β_λ	8.99	25.11	74.95	111.94
β_x	−18.66	−30.76	−114.74	−145.86
β_y	18.56	31.48	1.60	−3.57
β_z	0.20	3.22	0.12	1.23
$\beta_{tot}(\lambda)$	26.32	44.13	114.75	145.91
		$\lambda = 0$ (Static)		
$\mu\beta_0$[b]	9.83	31.0	137.34	258.16
β_0	3.97	9.02	39.35	49.43
β_x	−8.53	−10.53	−61.87	−63.21
β_y	8.34	14.44	−0.53	0.14
β_z	0.03	1.31	−0.02	1.24
$\beta_{tot}(0)$	11.93	17.92	61.87	63.22

[a] Hyperpolarizabilities are given in 10^{-30} esu, and the $\mu\beta_{\lambda,0}$ products are given in 10^{-48} esu. [b] Evaluated using the computed B3LYP/6-31G** dipole moments (see Table 4).

applications[60] has values of $\mu\beta_\lambda = 525 \times 10^{-48}$ esu at the same wavelength as that used in our measurements (λ = 1.907 μm) and $\mu\beta_0 = 409 \times 10^{-48}$ esu (errors estimated to be ±15%).[60b]

The Zn complex shows the largest $\mu\beta_\lambda$ product, according to what was already evidenced by previous EFISH investigations on Schiff base complexes.[23,61] The other complexes are characterized by $\mu\beta_\lambda$ and β_λ values in the range normally observed for Schiff base complexes.[3,5] By comparing CuL^2 and NiL^2 complexes, which are structurally very similar and have virtually the same dipole moment, we note a strong decrease in β_λ on going from Cu to Ni, confirming that open-shell Schiff base complexes can have larger hyperpolarizability compared with the corresponding closed-shell ones.[3,61] On the other hand, it is quite surprising the low NLO response of VOL^2 as given by EFISH measurements, on account of the similarity with the other ML^2 complexes as inferred from their UV−vis spectra (see Table 5). This anomalous behavior deserves further investigation. Comparison between the $\mu\beta_\lambda$ values of ZnL^1 and those of ZnL^2 indicates the strong effect of the phenylazo group in favoring intramolecular charge transfer, though this chromophore does not appear to be a good electron acceptor in the ground state.

In all the examined cases, the EFISH $\mu\beta_\lambda$ values are negative; that is, the angle between the vector β_{tot} and the vector μ is greater than 90°. In the case of typical push−

(60) (a) Singer, K. D.; Sohn, J. E.; Lalama, S. J. *Appl. Phys. Lett.* **1986**, *49*, 248−250. (b) Singer, K. D.; Sohn, J. E.; King, L. A.; Gordon, H. M.; Katz, H. E.; Dirk, C. W. *J. Opt. Soc. Am. B* **1989**, *6*, 1339−1350.
(61) Ledoux, I.; Zyss, J. *Pure Appl. Opt.* **1996**, *5*, 603−612.

pull systems, this generally means that the two vectors are almost parallel and point toward opposite directions; that is, charge transfer occurs in the opposite direction with respect to the ground state polarization. In our complexes, only the direction of β_{tot} is well-defined; in fact, according to the simulations of electronic spectra for ML^2, charge transfer is unequivocally directed toward the phenylazo-salicylaldehyde moiety. Dipole moments, on the contrary, are very small, and their direction is not easily predictable because the different molecular moieties are scarcely polar and not organized to give a well-defined charge asymmetry. As a matter of fact, however, the dipole vectors of all complexes are oriented in such a way that the projections of β_{tot} on them are negative. On the other hand, calculations on Ni and Zn complexes predict positive $\mu\beta_\lambda$ values (see Table 8 and Figure 6). This disagreement can be presumably ascribed to the incorrect evaluation of the *direction* of μ. We have already outlined the significant role played on the dipole of Zn complexes by the coordinated methanol molecule. Solvent effects may modify its orientation with respect to the complex so that the effective dipole orientation can be significantly different from that determined for the simulated gas-phase system. Similar considerations can be made for Ni complexes, for which the presence of coordinated solvent molecules cannot be a priori excluded. A detailed investigation of such effects, which requires geometry optimizations in solution rather than in vacuo, is deferred to future work.[62]

Apart from the discrepancy concerning the sign of the $\mu\beta_\lambda$ values, theoretical calculations are able to predict the general trend of the EFISH $\mu\beta_\lambda$ values for the closed-shell complexes. They confirm that Zn gives a greater NLO response with respect to Ni, independent of the ligand, and predict a β_λ enhancement of about 4 (3 from EFISH measurements) on going from the L^1 to the L^2 ligand. An even greater β_λ enhancement, equal to 8, is determined by the phenylazo group for the Ni complexes.

Via theoretical calculations, we are able to evaluate, through the β_i components, the principal directions and magnitudes of charge transfer within the complexes. In the case of ML^1 complexes, a similar degree of charge transfer occurs along the *x* and *y* axes, while for ML^2 complexes, only the *x* component is observed according to what was predicted by the simulated spectra. Furthermore, we can get information on the effect of frequency on the NLO response by comparing, for example, the β_{tot} magnitudes computed at the experimental frequency, $\beta_{tot}(\lambda)$, with the static ones, $\beta_{tot}(0)$. The enhancement factor, $\beta_{tot}(\lambda)/\beta_{tot}(0)$, computed for Zn complexes (2.5 and 2.3 for ZnL^1 and ZnL^2, respectively) is greater than that obtained for Ni complexes (2.2 and 1.9 for NiL^1 and NiL^2, respectively).

(62) Preliminary work on ZnL^1 coordinated by one methanol molecule seems to confirm this hypothesis. Geometry optimization with solvent effects described through the COSMO model, using the Gaussian program, leads to a structure where the methanol is slightly rotated with respect to the in vacuo structure. Accordingly, the dipole moment undergoes a slight rotation approaching the experimental direction, though the entity of such a rotation is still too small to invert the sign of the $\mu\beta_\lambda$ product.

Conclusions

New unsymmetrical Schiff base complexes of Ni(II), Cu(II), Zn(II), and VO(II) based on *S*-methylisothiosemicarbazide have been synthesized and characterized. We have considered two ligands, which differ only for the presence of a phenylazo substituent on the salicylaldehyde moiety of the Schiff base contour. The possible application of this class of compounds as NLO materials has been tested for the first time through a combined experimental and theoretical study. The results of such investigation appear to be unexpectedly promising. EFISH measurements and TDDFT calculations, in fact, indicate that the NLO response of our complexes is competitive with that of the best organic and metallorganic candidates of similar size, though they do not possess the push−pull structure typical of most molecular materials for NLO applications. Moreover, TGA have demonstrated that these compounds show excellent thermal stability, unlike most Schiff base complexes. This property makes them suitable for an efficient utilization in technological applications.

The effect of the phenylazo group has been experimentally tested on the Zn complex, for which the magnitude of β_λ triplicates with respect to the unsubstituted compound. Theoretical calculations predicted for β_λ a similar (for the same complex) and even greater (for the Ni complex) enhancement factor associated with the presence of this chromophore. A comparison between complexes of different metals with the same phenylazo-substituted ligand indicated that the NLO response strongly depends upon the electronic configuration of the metal center, the largest β_λ value being obtained for the Zn complex. The different response of the metal complexes has been interpreted with the aid of TDDFT simulated spectra. In all cases, the predicted transitions are characterized by a large charge transfer principally directed toward the phenylazo-salicylaldehyde moiety and involving the metal atom in different ways. In particular, in Zn and VO complexes, the metal atom was found to be much less involved with respect to Ni and Cu complexes. Further work is planned to study in greater detail the role played by different transition metals in NLO properties of Schiff base complexes.

Acknowledgment. The authors thank Mr. F. De Zuane of CNR-ICIS for the magnetic susceptibility measurements. A.F. thanks the staff of the XRD1 beamline at the ELETTRA syncrotron (Trieste, Italy) for assistance. Data collection of complex **2** was performed during the "Workshop di Cristallografia Sperimentale ad Elettra" (Trieste, Oct. 24−26, 2000).

Supporting Information Available: Structural data for **2**, **3**, **4**, **7**, and **8** in CIF format, IR data of **1**−**8**, tables of the EI mass spectra of **1**−**8**, TGA curves of **1**−**8**. This material is available free of charge via the Internet at http://pubs.acs.org.

IC062035R